

Numerical approach to the dynamical Casimir effect

This article has been downloaded from IOPscience. Please scroll down to see the full text article.

2006 J. Phys. A: Math. Gen. 39 6711

(<http://iopscience.iop.org/0305-4470/39/21/S72>)

View [the table of contents for this issue](#), or go to the [journal homepage](#) for more

Download details:

IP Address: 171.66.16.105

The article was downloaded on 03/06/2010 at 04:34

Please note that [terms and conditions apply](#).

Numerical approach to the dynamical Casimir effect

Marcus Ruser

Département de Physique Théorique, Université de Genève, 24 quai Ernest Ansermet,
CH-1211 Genève 4, Switzerland

E-mail: Marcus.Ruser@physics.unige.ch

Received 10 November 2005, in final form 22 January 2006

Published 10 May 2006

Online at stacks.iop.org/JPhysA/39/6711

Abstract

The dynamical Casimir effect for a massless scalar field in 1+1-dimensions is studied numerically by solving a system of coupled first-order differential equations. The number of scalar particles created from vacuum is given by the solutions to this system which can be found by means of standard numerics. The formalism already used in a former work is derived in detail and is applied to resonant as well as off-resonant cavity oscillations.

PACS numbers: 11.10.–z, 42.50.Pq

1. Introduction

The possibility of creating photons out of vacuum fluctuations of the quantized electromagnetic field in dynamical cavities, the so-called dynamical Casimir effect (see [1] for a review), demonstrates the highly non-trivial nature of the quantum vacuum.

A scenario of particular interest are so-called vibrating cavities [2] where the distance between two parallel (ideal) mirrors changes periodically in time. The occurrence of resonance effects between the mechanical motion of the mirror and the quantum vacuum leading to (even exponentially) increasing occupation numbers in the resonance modes makes this configuration the most promising candidate for an experimental verification of this pure quantum effect.

Particle creation in one-dimensional vibrating cavities has been studied in numerous works [3–11]. When considering small amplitude oscillations, analytical results can be deduced showing that under resonance conditions the particle occupation numbers increase quadratically in time. Particle creation due to off-resonant wall motions has been investigated in, e.g., [8]. The evolution of the energy density in a one-dimensional cavity with one vibrating wall has also been studied by many authors [12–18] demonstrating that the total energy inside a resonantly vibrating cavity grows exponentially in time (see also [4]) while the total particle number increases only quadratically. Thus a pumping of energy into higher frequency modes takes place and particles of frequencies exceeding the mechanical frequency of the oscillating mirror are created. The energy for this process is provided by the energy which has to be given

to the system from outside to maintain the motion of the mirror against the radiation reaction force [19–22]. The more realistic case of a three-dimensional cavity is studied in [22–29]. Field quantization inside cavities with non-perfect boundary conditions has been investigated in, e.g., [30, 31] and corrections due to finite temperature effects are treated in [32–34]. The question of how the quantum vacuum interacts with the (classical) dynamics of the cavity has been addressed in [12, 35–37].

In this work, we present a formalism allowing for numerical investigation of the dynamical Casimir effect for scalar particles in a one-dimensional cavity. (For related numerical work see also [38–40].) We introduce a particular parametrization for the time evolution of the field modes yielding a system of coupled first-order differential equations. The solutions to this system determine the number of created particles and can be obtained by means of standard numerics. We employ the formalism to investigate the creation of real massless scalar particles in a resonantly as well as off-resonantly vibrating cavity and compare the numerical results with analytical predictions. These results are complementary to those already presented in [41].

With this formalism at hand the dynamical Casimir effect can be investigated fully numerically making it possible to study a variety of scenarios where no analytical results are known (large amplitude oscillations, arbitrary wall motions etc). Of special interest is of course the realistic case of the electromagnetic field in a three-dimensional cavity. Being easily extendable to arbitrary space dimensions the presented formalism can be used also in this case. In particular it allows us to calculate numerically the TE-mode contribution [27] to the photon creation taking the influence of the intermode coupling fully into account [43]. Hence the formalism can be used to cross-check analytical results also in this realistic case which might be of importance for future experiments. Let us finally note that the tools (and the numerical formalism presented here) used to study the dynamical Casimir effect can also be employed to investigate graviton generation in braneworld cosmology [42].

2. Hamiltonian and equations of motion

We consider the Hamilton operator

$$\hat{H}(t) = \frac{1}{2} \sum_n [\hat{p}_n^2 + \Omega_n^2(t) \hat{q}_n^2] - \frac{1}{2} \sum_{nm} M_{nm}(t) [\hat{q}_n \hat{p}_m + \hat{p}_m \hat{q}_n] \quad (1)$$

with

$$\hat{p}_n = \dot{\hat{q}}_n + \sum_m \hat{q}_m M_{mn}(t) \quad \text{and} \quad M_{nm}(t) = \int_{I(t)} dx \dot{\phi}_n(t, x) \phi_m(t, x) \quad (2)$$

describing the dynamics of a massless real scalar field $\Phi = \Phi(t, x)$ on a time-dependent interval $I(t) = [0, l(t)]$ in terms of the canonical operators \hat{q}_n and \hat{p}_n subject to the usual equal-time commutation relations. The corresponding canonical variables q_n and p_n are introduced via the expansion $\Phi(t, x) = \sum_n q_n(t) \phi_n(t, x)$ of the field and its momentum $\Pi(t, x) = \sum_n p_n(t) \phi_n(t, x)$ in time-dependent (instantaneous) eigenfunctions $\phi_n(t, x)$ satisfying the eigenvalue equation

$$-\partial_x^2 \phi_n(t, x) = \Omega_n^2(t) \phi_n(t, x) \quad (3)$$

on $I(t)$ with time-dependent eigenvalues $\Omega_n^2(t)$ [7]. The overdot denotes the derivative with respect to time t and we are using units with $\hbar = c = 1$. The time-dependent so-called coupling matrix M_{nm} arises due to the time-dependent boundary condition for the field at

$x = l(t)$ enforcing the eigenfunctions of $-\partial_x^2$ to be time-dependent. We take the boundary conditions at $x = 0$ and $x = l(t)$ to be of the form

$$[a_1 \Phi + a_2 \partial_x \Phi]|_{x=0} = [b_1 \Phi + b_2 \partial_x \Phi]|_{x=l(t)} = 0 \quad \forall t \quad (4)$$

with constants a_1, a_2, b_1 and b_2 ensuring that the set of eigenfunctions $\{\phi_n(t, x)\}$ is complete and orthonormal for all times.

Adopting the Heisenberg picture, the equations of motion for $\hat{q}_n(t)$ read [4, 7]

$$\ddot{\hat{q}}_n + \Omega_n^2 \hat{q}_n + \sum_m [M_{mn} - M_{nm}] \dot{\hat{q}}_m + \sum_m [\dot{M}_{mn} - N_{nm}] \hat{q}_m = 0 \quad (5)$$

where $N_{nm} = \sum_k M_{nk} M_{mk}$. The structure of the intermode coupling mediated by the coupling matrix M_{nm} depends on the particular kind of boundary conditions which decide on the specific form of the instantaneous eigenfunctions $\phi_n(t, x)$. It is worth noting that the Hamiltonian (1) does not correspond to the energy of the field because the coupling term does not contribute to the total energy defined via the energy momentum tensor [7]. From the Hamiltonian (1) and the equations of motion (5) we identify two external time dependences in the equations which will lead to particle creation: (i) the time-dependent eigenfrequencies $\Omega_n(t)$ and (ii) the coupling matrix $M_{nm}(t)$, called the squeezing and acceleration effect, respectively.

3. Vacuum and particle definition

Let us assume that the motion of the wall is switched on at $t = 0$ with $l(t)$ following a prescribed trajectory for a duration t_1 , ceases afterwards and is at rest again. Before and after the motion the coupling matrix vanishes and the time evolution of the operator \hat{q}_n is determined by the equation of an harmonic oscillator with constant frequency $\Omega_n^0 \equiv \Omega_n(t \leq 0)$ and $\Omega_n^1 \equiv \Omega_n(t \geq t_1)$, respectively¹. The corresponding Hamilton operator describing the quantized field for $t \leq 0$ and $t \geq t_1$ can then be diagonalized by introducing time-independent annihilation and creation operators $\{\hat{a}_n, \hat{a}_n^\dagger\}$, corresponding to the particle notion for $t \leq 0$, and $\{\hat{A}_n, \hat{A}_n^\dagger\}$ associated with the particle notion for $t \geq t_1$ via²

$$t \leq 0: \quad \hat{q}_n(t) = \frac{\hat{a}_n e^{-i\Omega_n^0 t}}{\sqrt{2\Omega_n^0}} + \text{h.c.}, \quad \hat{p}_n(t) = i\sqrt{\frac{\Omega_n^0}{2}} \hat{a}_n^\dagger e^{i\Omega_n^0 t} + \text{h.c.}, \quad (6)$$

$$t \geq t_1: \quad \hat{q}_n(t) = \frac{\hat{A}_n e^{-i\Omega_n^1(t-t_1)}}{\sqrt{2\Omega_n^1}} + \text{h.c.}, \quad \hat{p}_n(t) = i\sqrt{\frac{\Omega_n^1}{2}} \hat{A}_n^\dagger e^{i\Omega_n^1(t-t_1)} + \text{h.c.} \quad (7)$$

The initial and final vacuum states $|0, t \leq 0\rangle$ and $|0, t \geq t_1\rangle$, respectively, are introduced as the ground states of the corresponding diagonal Hamilton operators:

$$\hat{H} = \sum_n \begin{cases} \Omega_n^0 [\hat{a}_n^\dagger \hat{a}_n + 1/2] & \text{with } \hat{a}_n |0, t \leq 0\rangle = 0 & \text{for } t \leq 0 \\ \Omega_n^1 [\hat{A}_n^\dagger \hat{A}_n + 1/2] & \text{with } \hat{A}_n |0, t \geq t_1\rangle = 0 & \text{for } t \geq t_1. \end{cases} \quad (8)$$

The set of initial-state operators $\{\hat{a}_n, \hat{a}_n^\dagger\}$ is related to the set of final-state operators $\{\hat{A}_n, \hat{A}_n^\dagger\}$ by a Bogoliubov transformation

$$\hat{A}_n = \sum_m [\mathcal{A}_{mn}(t_1) \hat{a}_m + \mathcal{B}_{mn}^*(t_1) \hat{a}_m^\dagger], \quad (9)$$

¹ Here the final position $l(t_1) = l_1$ is assumed to be arbitrary. In the case of a vibrating cavity it is natural to consider times t_1 after which the dynamical wall has returned to its initial position.

² We are assuming that $\Omega_n^0 \neq 0$ and $\Omega_n^1 \neq 0$ for all n .

where $\mathcal{A}_{mn}(t_1)$ and $\mathcal{B}_{mn}(t_1)$ satisfy the relations

$$\sum_m [\mathcal{A}_{mn}\mathcal{A}_{mk}^* - \mathcal{B}_{mn}^*\mathcal{B}_{mk}] = \delta_{nk}, \quad \sum_m [\mathcal{A}_{mn}\mathcal{B}_{mk}^* - \mathcal{B}_{mn}^*\mathcal{A}_{mk}] = 0. \quad (10)$$

For $t \geq t_1$ the particle number operator $\hat{N}_n = \hat{A}_n^\dagger \hat{A}_n$ defined with respect to the final vacuum state counts the number of physical particles. The number of particles created in a mode n during the motion of the wall is given as the expectation value of \hat{N}_n with respect to the initial vacuum state $|0, t \leq 0\rangle$:

$$N_n(t_1) = \langle 0, t \leq 0 | \hat{N}_n | 0, t \leq 0 \rangle = \sum_m |\mathcal{B}_{mn}(t_1)|^2. \quad (11)$$

Accordingly, total particle number $N(t_1)$ and energy $E(t_1)$ of the motion induced radiation are given by

$$N(t_1) = \sum_n N_n(t_1), \quad E(t_1) = \sum_n \Omega_n^1 N_n(t_1). \quad (12)$$

Both quantities are in general ill defined and therefore require appropriate regularization. For a time dependence of the boundary $l(t)$ which is not sufficiently smooth, i.e. it exhibits discontinuities in its time-derivative appearing for instance when switching the motion on and off instantaneously, one may expect that part of the particle creation is due to this discontinuity in the velocity which may cause the excitation of modes of even arbitrary high frequencies. Hence a (large) contribution to the predicted particle creation may be spurious and in the case that arbitrary high frequency modes become excited the summations in (12) do not converge. This can be avoided most easily by introducing a frequency cut-off which effectively smoothes the dynamics $l(t)$. When calculating the quantities (12) numerically we will make use of such a frequency cut-off which is determined by the stability of the numerical results for single modes, i.e. stability of the expectation value (11) with respect to the cut-off. Note that an explicit frequency cut-off also accounts for imperfect (non-ideal) boundary conditions for high frequency modes [7].

4. Time evolution

During the motion of the boundary some or even infinitely many modes may be coupled. For $t \geq 0$ the operators $\hat{q}_n(t)$ and $\hat{p}_n(t)$ given by $\hat{U}^\dagger \hat{q}_n(0) \hat{U}$ and $\hat{U}^\dagger \hat{p}_n(0) \hat{U}$, respectively, with $\hat{U} \equiv \hat{U}(t, 0) = \mathcal{T} \exp(-i \int_0^t dt' \hat{H}(t'))$ and \mathcal{T} denoting the time-ordering operator, can be expanded in initial state operators $\hat{a}_n, \hat{a}_n^\dagger$ and complex functions $\epsilon_n^{(m)}(t)$:

$$\hat{q}_n(t \geq 0) = \hat{U}^\dagger \hat{q}_n(0) \hat{U} = \sum_m \frac{\hat{a}_m}{\sqrt{2\Omega_m^0}} \epsilon_n^{(m)}(t) + \text{h.c.}, \quad (13)$$

$$\hat{p}_n(t \geq 0) = \hat{U}^\dagger \hat{p}_n(0) \hat{U} = \sum_m \frac{\hat{a}_m}{\sqrt{2\Omega_m^0}} \left[\dot{\epsilon}_n^{(m)}(t) + \sum_k M_{kn}(t) \epsilon_k^{(m)}(t) \right] + \text{h.c.} \quad (14)$$

By using the Heisenberg equation $\dot{\hat{O}}(t) = i[\hat{H}(t), \hat{O}(t)] + (\partial \hat{O}(t) / \partial t)_{\text{expl}}$, it is straightforward to show that the functions $\epsilon_n^{(m)}(t)$ satisfy the same differential equation (5) as $\hat{q}_n(t)$. Note that insertion of equation (13) into the mode expansion for Φ leads to the decomposition of the field used in, e.g., [4, 6, 8]. Through the formal expansion (13) we have reduced the problem of finding the time evolution for the operator $\hat{q}_n(t)$ to the problem of solving the system of coupled second-order differential equations (5) for $\epsilon_n^{(m)}(t)$. Demanding that equations (13)

and (14) have to match with the corresponding expressions (6) at $t = 0$ leads to the initial conditions

$$\epsilon_n^{(m)}(0) = \delta_{nm}, \quad \dot{\epsilon}_n^{(m)}(0) = -i\Omega_n^0 \delta_{nm} - M_{mn}(0). \quad (15)$$

Hence with $M_{mn}(0)$ vanishing only if $\dot{l}(0) = 0$ the initial condition $\dot{\epsilon}_n^{(m)}(0)$ is not simply $-i\Omega_n^0 \delta_{nm}$ when dealing with boundary motions $l(t)$ which have a discontinuity in the velocity at $t = 0$. Matching (7) with (13) and (14) at $t = t_1$ one finds

$$\mathcal{A}_{mn}(t_1) = \frac{1}{2} \sqrt{\frac{\Omega_n^1}{\Omega_m^0}} \left\{ \epsilon_n^{(m)}(t_1) + \frac{i}{\Omega_n^1} \left[\dot{\epsilon}_n^{(m)}(t_1) + \sum_k M_{kn}(t_1) \epsilon_k^{(m)}(t_1) \right] \right\} \quad (16)$$

$$\mathcal{B}_{mn}(t_1) = \frac{1}{2} \sqrt{\frac{\Omega_n^1}{\Omega_m^0}} \left\{ \epsilon_n^{(m)}(t_1) - \frac{i}{\Omega_n^1} \left[\dot{\epsilon}_n^{(m)}(t_1) + \sum_k M_{kn}(t_1) \epsilon_k^{(m)}(t_1) \right] \right\}. \quad (17)$$

Starting with the initial vacuum $|0, t \leq 0\rangle$ the Bogoliubov transformation (9) has to become trivial for $t_1 = 0$, i.e. $\hat{A}_k = \hat{a}_k$, implying the vacuum initial conditions

$$\mathcal{A}_{mn}(0) = \delta_{mn} \quad \text{and} \quad \mathcal{B}_{mn}(0) = 0 \quad (18)$$

which are consistent with the initial conditions (15). The emergence of $M_{mn}(0)$ in the initial conditions (15) therefore guarantees to meet the vacuum initial conditions when the motion of the boundary starts instantaneously with a nonzero velocity.

By introducing the auxiliary functions³

$$\xi_n^{(m)}(t) = \epsilon_n^{(m)}(t) + \frac{i}{\Omega_n^0} \left[\dot{\epsilon}_n^{(m)}(t) + \sum_k M_{kn}(t) \epsilon_k^{(m)}(t) \right], \quad (19)$$

$$\eta_n^{(m)}(t) = \epsilon_n^{(m)}(t) - \frac{i}{\Omega_n^0} \left[\dot{\epsilon}_n^{(m)}(t) + \sum_k M_{kn}(t) \epsilon_k^{(m)}(t) \right] \quad (20)$$

expressions (16) and (17) can be rewritten as

$$\mathcal{A}_{mn}(t_1) = \frac{1}{2} \sqrt{\frac{\Omega_n^1}{\Omega_m^0}} \left[\Delta_n^+(t_1) \xi_n^{(m)}(t_1) + \Delta_n^-(t_1) \eta_n^{(m)}(t_1) \right], \quad (21)$$

$$\mathcal{B}_{mn}(t_1) = \frac{1}{2} \sqrt{\frac{\Omega_n^1}{\Omega_m^0}} \left[\Delta_n^-(t_1) \xi_n^{(m)}(t_1) + \Delta_n^+(t_1) \eta_n^{(m)}(t_1) \right] \quad (22)$$

with

$$\Delta_n^\pm(t) = \frac{1}{2} \left[1 \pm \frac{\Omega_n^0}{\Omega_n(t)} \right]. \quad (23)$$

The quantity $\Delta_n^\pm(t_1)$ is a measure for the deviation of the final state of the cavity, characterized by the cavity length $l(t_1)$, with respect to its initial size l_0 . If at time t_1 the cavity size is equal to the initial size l_0 , for instance in the important case that t_1 is a multiple of the period of oscillations of the cavity, we have $\mathcal{B}_{mn}(t_1) = (1/2) \sqrt{\Omega_n^0/\Omega_m^0} \eta_n^{(m)}(t_1)$ and therefore $N_n(t_1) = (1/4) \sum_m (\Omega_n^0/\Omega_m^0) |\eta_n^{(m)}(t_1)|^2$.

³ A derivation can be found in appendix A.

The advantage of introducing the functions $\xi_n^{(m)}$ and $\eta_n^{(m)}$ is that they satisfy the following system of first-order differential equations:

$$\dot{\xi}_n^{(m)} = -i[a_{nn}^+ \xi_n^{(m)} - a_{nn}^- \eta_n^{(m)}] - \sum_k [c_{nk}^- \xi_k^{(m)} + c_{nk}^+ \eta_k^{(m)}], \quad (24)$$

$$\dot{\eta}_n^{(m)} = -i[a_{nn}^- \xi_n^{(m)} - a_{nn}^+ \eta_n^{(m)}] - \sum_k [c_{nk}^+ \xi_k^{(m)} + c_{nk}^- \eta_k^{(m)}] \quad (25)$$

with

$$a_{nn}^\pm(t) = \frac{\Omega_n^0}{2} \left\{ 1 \pm \left[\frac{\Omega_n(t)}{\Omega_n^0} \right]^2 \right\} \quad \text{and} \quad c_{nk}^\pm(t) = \frac{1}{2} \left[M_{kn}(t) \pm \frac{\Omega_k^0}{\Omega_n^0} M_{nk}(t) \right]. \quad (26)$$

Besides the time-dependent frequency $\Omega_n(t)$, only the coupling matrix $M_{kn}(t)$ enters into this system of coupled differential equations but neither $N_{nk}(t)$ nor its time derivative $\dot{M}_{kn}(t)$. The vacuum initial conditions (18) entail the initial conditions for the functions $\xi_n^{(m)}$ and $\eta_n^{(m)}$ to be

$$\xi_n^{(m)}(0) = 2\delta_{mn} \quad \eta_n^{(m)}(0) = 0. \quad (27)$$

Let us stress that all derivations and equations shown so far, do not rely on particular symmetry properties of the coupling matrix.

By means of equation (22) the number of particles created from vacuum during the dynamics of the cavity as well as the associated energy may now be calculated from the solutions $\xi_n^{(m)}$ and $\eta_n^{(m)}$ of the system of coupled first-order differential equations formed by equations (24) and (25).

In order to obtain the numerical results presented in the next section we proceed in the following way: a cut-off parameter k_{\max} is introduced to make the system of differential equations finite and suitable for a numerical treatment. The system of coupled differential equations is then evolved numerically from $t = 0$ up to a final time t_{\max} and the expectation value (11) is calculated for several times in between. By doing so we interpret t_1 as a continuous variable such that equation (11) becomes a continuous function of time⁴. Consequently, the stability of the numerical solutions with respect to the cut-off has to be ensured. In particular k_{\max} will be chosen such that the numerical results for the number of particles created in single modes (11) are stable. Furthermore, the quality of the numerical results is assessed by testing the relations Bogoliubov (10).

This procedure is of course not without problems when the expectation values are evaluated also for times t_1 at which $\dot{l}(t_1) \neq 0$. The used particle definition requires then a matching of the solutions to expressions corresponding to the static configuration with $\dot{l}(t_1) = 0$, hence a discontinuity in the velocity appears which may cause spurious effects. However the cut-off automatically ensures that possible spurious effects do not yield a divergent total particle number (see also section 3). Indeed we will see that in the particular scenario of interest—vibrating cavity—the influence of this matching problem is tiny and the numerical results agree perfectly with analytical predictions.

5. Numerical results and discussion

In this section we consider a massless real scalar field subject to Dirichlet boundary conditions at $x = 0, l(t)$ and the much studied sinusoidal cavity motion

$$l(t) = l_0[1 + \epsilon \sin(\omega t)], \quad \epsilon \ll 1. \quad (28)$$

⁴ Interpreting t_1 as a continuous function of time one can of course derive a corresponding system of coupled differential equations for \mathcal{A}_{mn} and \mathcal{B}_{mn} (see appendix B).

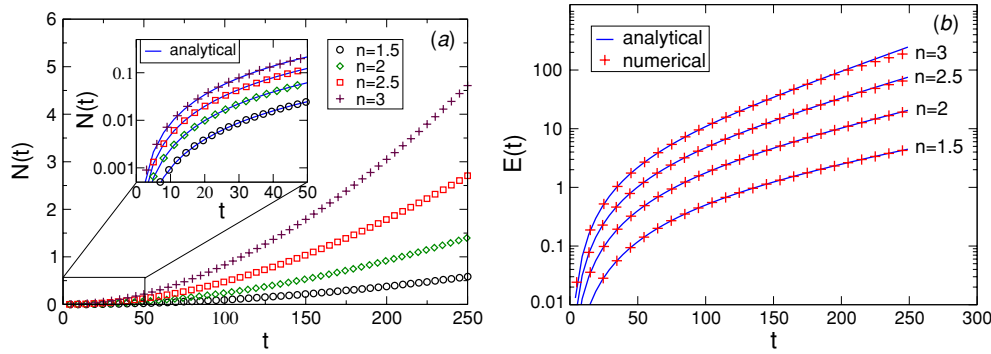


Figure 1. (a) Total number of particles produced in a cavity vibrating with (28) and $\omega = 2n\pi$ with $n = 1.5, 2, 2.5$ and 3 . The small plot shows the results in the time range $[0, 50]$ together with the analytical prediction (solid line) $N(t) = n(4n^2 - 1)(10^{-3}\pi t)^2/12$ of [6, 8] valid for short times ($10^{-3}\pi t \ll 1$). (b) Numerical results for the created energy $E(t)$ corresponding to (a) together with the analytical prediction $E(t) = (4n^2 - 1)\pi \sinh^2(n10^{-3}\pi t)/12$ of [8] (solid line). The results correspond to the largest cut-off parameters as given in figure 2.

The time-dependent frequency and coupling matrix are given by [7]

$$\Omega_n(t) = \frac{n\pi}{l(t)}, \quad M_{nm} = \frac{\dot{l}(t)}{l(t)} (-1)^{n+m} \frac{2nm}{m^2 - n^2} \quad (29)$$

for $n \neq m$ and $M_{nn}(t) = 0$ with $n, m = 1, 2, 3, \dots$. The motion (28) whose absolute value of the velocity is maximal at the beginning of the motion as well as for times at which the wall returns to its initial position features the above described matching problem. In [41] we have already studied particle creation caused by this motion for the main resonance case $\omega = 2\Omega_1^0$ with the same formalism. We have found that for sufficiently small ϵ and appropriate k_{\max} the numerical results are in excellent agreement with analytical predictions of [3, 4]. Furthermore, the influence of the initial discontinuity in the velocity of the motion (28) has been investigated showing that it is negligible for $\epsilon \ll 1$.

Here we want to concentrate on higher resonances $\omega = 2\Omega_n^0$ with $n > 1$ and off-resonant frequencies (detuning). In the simulations we set $l_0 = 1$ and $\epsilon = 0.001$. For these parameters it is shown in [41] that the numerical results agree very well with analytical predictions derived under the assumption $\epsilon \ll 1$. The numerical results are compared with analytical expressions obtained in [6, 8]. Remarks about the numerics can be found in appendix C.

In figure 1(a), we show the numerical results for the total particle number in the time range $[0, 250]$ for resonant cavity frequencies $\omega = 2\Omega_n^0 = 2n\pi$ for $n = 1.5, 2, 2.5$ and 3 and the associated energy of the created quantum radiation is depicted in figure 1(b). The corresponding particle spectra are shown in figure 2 for different cut-off parameters k_{\max} to demonstrate numerical stability of the results. Here stability of the numerical results means that for the lowest modes k the value $N_k(t)$ remains unchanged (within numerical precision) under variation of k_{\max} . The spectra confirm that no modes $k = 2np$ with $p = 1, 2, 3, \dots$ are coupled (and therefore excited) as predicted by the coupling condition $\omega = |\Omega_k^0 \pm \Omega_l^0|$ derived and discussed in [23].

For short times $\epsilon\pi t = 10^{-3}\pi t \ll 1$, the numerical results are well described by the analytical predictions of [6, 8]. The numerically calculated spectra for times $t = 25$ shown in figure 2 are well fitted by the analytical expression $N_k(t) = (2n - k)k(10^{-3}\pi t)^2/4$ for $k < 2n$ and $N_k(t) = 0$ otherwise [6], predicting a parabolic shape of the particle spectrum. More quantitatively, for $n = 2$, for instance, the predicted values $N_1(t) =$

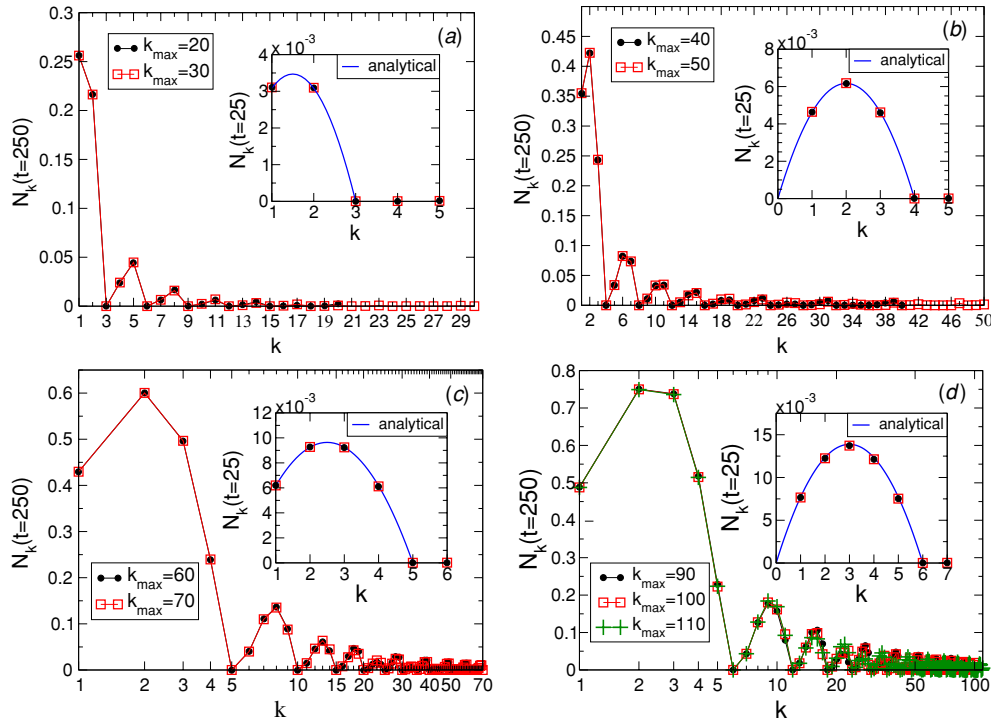


Figure 2. Particle spectra for (a) $\omega = 3\pi$, (b) $\omega = 4\pi$, (c) $\omega = 5\pi$ and (d) $\omega = 6\pi$ corresponding to the results shown in figure 1. The small plots compare the numerical results for $N_k(t = 25)$ with the analytical prediction $N_k(t) = (2n - k)k(10^{-3}\pi t)^2/4$ of [6] plotted for continuous values of k (solid line).

$25) = N_3(t = 25) \sim 4.63 \times 10^{-3}$, $N_2(t = 25) = 6.17 \times 10^{-3}$ agree well with the values $N_1(t = 25) = 4.62 \times 10^{-3}$, $N_2(t = 25) = 6.14 \times 10^{-3}$ and $N_3(t = 25) = 4.59 \times 10^{-3}$ obtained from the numerical simulations with $k_{\max} = 50$. Consequently, the total number of created particles is perfectly described by the expression $N(t) = n(4n^2 - 1)(10^{-3}\pi t)^2/12$ [6, 8] as is demonstrated in the small plot in figure 1(a).

For the entire integration range $[0, 250]$ we compare the numerical results for the total energy associated with the created quantum radiation with the analytical expression $E(t) = (4n^2 - 1)\pi \sinh^2(n10^{-3}\pi t)/12$ [8] predicting that the energy increases exponentially with time (figure 1(b)). The numerical values and the analytical prediction agree very well for $n = 1.5$ and 2. In the case of $n = 2.5$ and 3 we observe slight deviations towards the end of the integration range. This is due to the numerical instabilities in the corresponding particle spectra (cf figures 2(c) and (d)). The numerical values for N_k with k larger than some value ($k > 10$ for $n = 3$, for instance) do not remain unchanged when varying k_{\max} . Even N_k is small for the higher frequencies compared to the values of N_k for the excited lowest modes their contribution to the total energy is significant because of their high frequency. Hence relatively small instabilities in N_k for larger k give rise to a non-stable (with respect to k_{\max}) result for the energy. In order to gain better agreement of the numerical results for the energy for $n = 2.5$ and 3 with the analytical prediction a further increase of k_{\max} is necessary.

We now consider the case of detuning $\omega = 2\pi(n + \delta n)$. In an off-resonant vibrating one-dimensional cavity the total energy associated with the created particles may increase exponentially $E(t) = (\pi/12)(4n^2 - 1) \sinh^2(n\sqrt{1 - \gamma^2}\pi 10^{-3}t)/(1 - \gamma^2)$

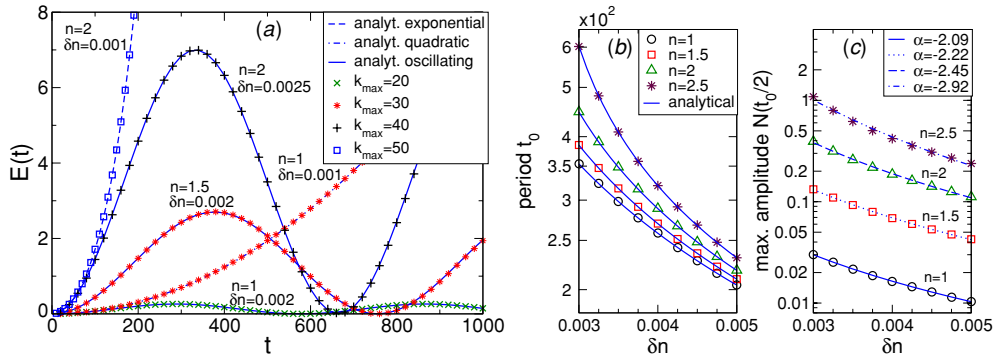


Figure 3. (a) Energy associated with the particles created in an off-resonantly vibrating one-dimensional cavity. Numerical results are compared to the analytical predictions of [8]. The numerical results are always shown for cut-off parameters k_{\max} which ensure numerical stability. (b) Period of particle number oscillations caused by detuning. The numerically obtained period is compared with the analytical prediction $t_0 = 10^3/(n\sqrt{\gamma^2 - 1})$ of [8]. (c) Maximal amplitude $N(t_0/2)$ of the corresponding particle number oscillations fitted to the power law $N(t_0/2) \propto (\delta n)^\alpha$.

if $\gamma < 1$, quadratically $E(t) = (\pi/3)(4n^2 - 1)(n\pi 10^{-3}t/2)^2$ if $\gamma = 1$ or oscillate $E(t) = (\pi/12)(4n^2 - 1)\sin^2(n\sqrt{\gamma^2 - 1}\pi 10^{-3}t)/(\gamma^2 - 1)$ if $\gamma > 1$, depending on the strength of detuning δn parametrized by $\gamma = \delta n \times 10^3/n$ [8]. In figure 3(a) results for the total energy obtained in simulations with different off-resonant frequencies are shown covering all three different possibilities for γ and compared to the analytical predictions. In all cases the numerical results are very well described by the analytical expressions. Figure 3(b) depicts the periods of the energy (and particle number) oscillations as obtained from the simulations and compares them with the analytical prediction $t_0 = 10^3/(n\sqrt{\gamma^2 - 1})$ showing that both are in good agreement. The numerical values for the maximal amplitudes $N(t_0/2)$ of the corresponding particle number oscillations are shown in figure 3(c) and fitted to the power law $N(t_0/2) \propto (\delta n)^\alpha$ with values of α as indicated in the figure.

The numerical results presented in this section are entirely in very good agreement with the corresponding analytical predictions derived for small amplitude oscillations $\epsilon \ll 1$ which demonstrates the reliability of the numerical simulations. However, a few critical comments are in order. In our considerations above, the analytical expressions have been treated as continuous functions of time. But strictly speaking, they are valid only for times at which the moving wall has returned to its initial position. Moreover, in the numerical simulations the expectation values have been calculated also for times at which the velocity of the moving wall is nonzero (matching problem). Consequently one may expect that part of the particle production is spurious and in particular if modes of arbitrarily high frequency are excited, for instance due to the initial discontinuity in the velocity of the motion (28), and $k_{\max} \rightarrow \infty$ the particle number diverges and the numerical results do not agree with the analytical predictions. In the numerical simulations this is automatically avoided due to the cut-off k_{\max} . Nevertheless, working with a finite cut-off is well motivated because it simulates imperfect boundary conditions for high frequency modes and, as a matter of course, is a necessity for a numerical treatment. For the numerical results presented above, these spurious effects are negligibly small and therefore the numerical results agree very well with the analytical predictions. This is due to the fact that we restrict ourselves to small amplitudes $\epsilon \ll 1$ and hence to small velocities. Therefore the effect of the discontinuity in the velocity of the boundary motion on the particle creation is expected to be small. This has been studied

for the initial discontinuity in the velocity in [41] in detail demonstrating that the matching problem becomes only important for larger ϵ . In appendix C we discuss the convergence of the numerical results in comprehension with the numerical accuracy of the simulations for the case $\omega = 3\pi$ more detailed.

6. Conclusion

A formalism allowing for numerical investigation of particle creation from vacuum in dynamical cavities, i.e. the dynamical Casimir effect, has been presented. By introducing a particular parametrization for the time-evolution of the field modes inside the dynamical cavity, a system of coupled first-order linear differential equations has been derived. Physical quantities such as the number of particles created during the dynamics of the cavity and the associated energy are determined by the solutions to this system which can be found by applying standard numerics.

In continuation of the work [41] we have studied the creation of massless scalar particles due to resonant as well as off-resonant sinusoidal oscillations of one of the cavity walls. The numerical results are entirely in agreement with the analytical predictions derived in [6, 8] demonstrating that the numerical simulations are reliable and the method introduced is appropriate to study the dynamical Casimir effect fully numerically.

Potential problems inherent in the method, in particular the matching problem due to discontinuities in the velocity of the boundary motion yielding spurious contributions to the total particle number, have been discussed. It has been shown that this effect is negligibly small for cavity vibrations with a sufficiently small amplitude.

Being derived very generally, the method is applicable for different kinds of boundary conditions of the form (4) provided that the spectrum $\{\Omega_n\}$ contains no zero mode, i.e. $\Omega_n > 0 \forall n$ and can easily be extended to massive scalar fields by substituting for the frequency Ω_n the corresponding expression for a massive scalar field, i.e. $\Omega_n = \sqrt{(n\pi)^2/L^2 + m^2}$ where m is the mass. Furthermore, the generalization to higher dimensional cavities is straightforward. This makes it possible to study the dynamical Casimir effect for a variety of possible interesting scenarios where less or even nothing is known analytically. As already mentioned in the introduction, TE-mode photon creation in a three-dimensional rectangular cavity [23] can be studied with the same method as well because it can be related to the production of massive scalar particles in a one-dimensional cavity [43]. However, more complicated boundary conditions than (4) appearing for example when studying TM-mode photons [27] cannot be treated within this approach.

Acknowledgments

The author would like to thank Ruth Durrer for comments on the manuscript as well as Diego Dalvit and Francisco Mazzitelli for discussions during the QFEXT'05 workshop and Emilio Elizalde for organizing it. Financial support from the Swiss National Science Foundation is gratefully acknowledged.

Appendix A. Derivation of $\xi_n^{(m)}$ and $\eta_n^{(m)}$

The auxiliary functions $\xi_n^{(m)}(t)$ and $\eta_n^{(m)}(t)$ (equations (19) and (20)) can be introduced in the following way: define an operator $\hat{b}_n(t)$ via $\hat{b}_n(t) := \hat{U}^\dagger(t, 0)\hat{a}_n\hat{U}(t, 0)$ with \hat{a}_n being the annihilation operator corresponding to the initial state (equation (6)), i.e. $\hat{a}_n =$

$(1/\sqrt{2})[\sqrt{\Omega_n^0}\hat{q}_n(0) + (i/\sqrt{\Omega_n^0})\hat{p}_n(0)]$. Hence $\hat{b}_n(t) = (1/\sqrt{2})[\sqrt{\Omega_n^0}\hat{U}^\dagger(t, 0)\hat{q}_n(0)\hat{U}(t, 0) + (i/\sqrt{\Omega_n^0})\hat{U}^\dagger(t, 0)\hat{p}_n(0)\hat{U}(t, 0)]$. By using equations (13) and (14) one derives

$$\hat{b}_n(t \geq 0) = \sum_m \frac{1}{2} \sqrt{\frac{\Omega_n^0}{\Omega_m^0}} [\xi_n^{(m)}(t)\hat{a}_m + \eta_n^{(m)*}(t)\hat{a}_m^\dagger] \quad (\text{A.1})$$

with $\xi_n^{(m)}(t)$ and $\eta_n^{(m)}(t)$ defined in equations (19) and (20). Note that this definition of the time evolution for $\hat{b}_n(t)$ does not account for an explicit time-dependence of $\hat{b}_n(t)$. Therefore, in general, no meaningful notion of particles may be assigned to the operator $\hat{b}_n(t)$. This manifests itself in the relation between the operator \hat{A}_n corresponding to the particle notion for $t \geq t_1$ (equation (7)) and the operators $\hat{b}_n(t_1)$, $\hat{b}_n^\dagger(t_1)$ given by

$$\hat{A}_n = \sqrt{\frac{\Omega_n^1}{\Omega_n^0}} [\Delta_n^+(t_1)\hat{b}_n(t_1) + \Delta_n^-(t_1)\hat{b}_n^\dagger(t_1)] \quad (\text{A.2})$$

with $\Delta_n^\pm(t)$ defined in (23). Equation (A.2) follows directly from equation (9) with (21), (22) and (A.1). For motions ending at $t = t_1$ with $l(t_1) \neq l_0$ the operator $\hat{b}_n(t)$ has not evolved into the operator \hat{A}_n associated with the correct particle notion after the dynamics. However, if $l(t_1) = l_0$, for example when t_1 is a multiple of the period of boundary vibrations, $\hat{A}_n = \hat{b}_n(t_1)$.

Appendix B. The system for $\mathcal{A}_n^{(m)}$ and $\mathcal{B}_n^{(m)}$

Taking the stopping time t_1 in (16) and (17) to be a continuous variable one derives the following system of coupled differential equations for \mathcal{A}_{mn} and \mathcal{B}_{mn} :

$$\dot{\mathcal{A}}_{mn} = -i\Omega_n \mathcal{A}_{mn} + \Gamma_n \mathcal{B}_{mn} + \sum_k [K_{nk}^- \mathcal{A}_{mk} - K_{nk}^+ \mathcal{B}_{mk}] \quad (\text{B.1})$$

$$\dot{\mathcal{B}}_{mn} = -i\Omega_n \mathcal{B}_{mn} + \Gamma_n \mathcal{A}_{mn} + \sum_k [K_{nk}^- \mathcal{B}_{mk} - K_{nk}^+ \mathcal{A}_{mk}] \quad (\text{B.2})$$

with

$$\Gamma_n(t) = \frac{1}{2} \frac{\dot{\Omega}_n(t)}{\Omega_n(t)} \quad K_{nk}^\pm(t) = \frac{1}{2} \left[\sqrt{\frac{\Omega_k(t)}{\Omega_n(t)}} M_{nk}(t) \pm \sqrt{\frac{\Omega_n(t)}{\Omega_k(t)}} M_{kn}(t) \right]. \quad (\text{B.3})$$

Appendix C. Numerics

The numerical simulations have been performed by using a Runge–Kutta Prince–Dormand method (rk8pd) based on source code provided by the GNU Scientific Library (GSL) [44]. In the table in figure 4, we show the numerical values for the total number of particles $N(t)$ created in a cavity subject to sinusoidal oscillations of the form (28) with frequency $\omega = 3\pi$ (cf figures 1 and 2(a)) for two times $t = 249.5$ and $t = 250.0$ and cut-off parameters $k_{\max} = 20, 30, 40, 50$ and 60 . The plot in figure 4 shows the diagonal part of the first of the Bogoliubov relations (10) $d_k = 1 - \sum_m (|\mathcal{A}_{mk}|^2 - |\mathcal{B}_{mk}|^2) = 0$ for $k = 1, \dots, 10$ and $51, \dots, 60$ computed from the solutions of the simulation with $k_{\max} = 60$. The absolute and relative errors for the rk8pd routine in the simulations have been set to 10^{-8} .

The plot demonstrates that for those settings $d_k = 0$ is satisfied by the numerical solutions up to $\sim 3 \times 10^{-5}$ at the end of the integration range. Thereby the accuracy is better for the lowest modes $k = 1, \dots, 10$ than for the modes $k = 51, \dots, 60$. This is partly due to the fact

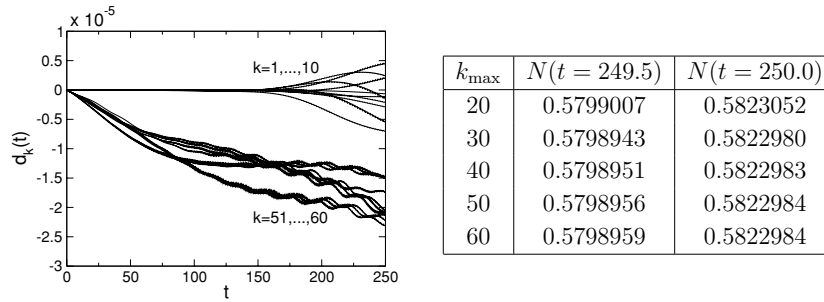


Figure 4. Left: plot showing the numerically evaluated diagonal part of the first of the Bogoliubov relations (10) $d_k = 1 - \sum_m (|\mathcal{A}_{mk}|^2 - |\mathcal{B}_{mk}|^2)$ for the lowest frequencies $k = 1, \dots, 10$ as well as $k = 51, \dots, 60$ corresponding to the simulation with cut-off $k_{\max} = 60$. Right: table showing the numerical values of the total particle number at times $t = 249.5$ and $t = 250$ obtained for $\omega = 3\pi$ and $k_{\max} = 20, 30, 40, 50$ and 60 .

that the higher modes are more affected by the truncation of the infinite system at $k_{\max} = 60$ than the lowest modes. The accuracy for the intermediate modes $k = 11, \dots, 50$ lies in between the two ‘bands’ visible in the plot. The remaining Bogoliubov relations are satisfied with at least the same accuracy demonstrating that the numerical errors are small compared to the values of the particle numbers itself. We consider d_k as the determining measure for the accuracy of the numerical calculations which can easily be enhanced further by increasing the preset accuracy of the integration routine.

The numerical values for $N(t = 249.5)$ and $N(t = 250.0)$ summarized in the table in figure 4 are shown with seven decimal places. Varying the cut-off between $k_{\max} = 30$ and 60 both values change only in the last two of the seven decimal places shown and therefore the variation in $N(t)$ when changing k_{\max} is smaller than 10^{-5} , i.e. smaller than the numerical error in the Bogoliubov relations. This demonstrates that the convergence of the numerical values for $N(t)$ is sufficiently good. Furthermore, because $\dot{l}(t = 250) = 3\pi\epsilon$ ($l_0 = 1$) we can conclude that spurious effects caused by discontinuities in the velocity (matching problem) are indeed negligibly small for the parameters considered ($\epsilon \ll 1$).

References

- [1] Dodonov V V 2001 Nonstationary Casimir effect and analytical solutions for quantum fields in cavities with moving boundaries *Modern Nonlinear Optics, Advances in Chemical Physics Series* vol 119, part 1, ed M W Evans (New York: Wiley) pp 309–94
- [2] Lambrecht A, Jaekel M-T and Reynaud S 1996 *Phys. Rev. Lett.* **77** 615
- [3] Dodonov V V, Klimov A B and Nikonov D E 1993 *J. Math. Phys.* **34** 2742
- [4] Dodonov V V and Klimov A B 1996 *Phys. Rev. A* **53** 2664
- [5] Dodonov V V 1996 *Phys. Lett. A* **213** 219
- [6] Ji J-Y, Jung H-H, Park J-W and Soh K-S 1997 *Phys. Rev. A* **56** 4440
- [7] Schützhold R, Plunien G and Soff G 1998 *Phys. Rev. A* **57** 2311
- [8] Dodonov V V 1998 *J. Phys. A: Math. Gen.* **31** 9835
- [9] Klimov A B and Altuzar V 1997 *Phys. Lett. A* **226** 41
- [10] Fu L-P, Duan C K and Guo G-C 1997 *Phys. Lett. A* **234** 163
- [11] Chizhov A V, Schrade G and Zubairy M S 1997 *Phys. Lett. A* **230** 269
- [12] Law C K 1994 *Phys. Rev. Lett.* **73** 1931
- [13] Cole C K and Schieve W C 1995 *Phys. Rev. A* **52** 4405
- [14] Méplan O and Gignoux C 1996 *Phys. Rev. Lett.* **76** 408
- [15] Dalvit D A R and Mazzitelli F D 1998 *Phys. Rev. A* **57** 2113

- [16] Wegrzyn P and Rog T 2001 *Acta Phys. Pol. B* **32** 129
- [17] Andreato M A and Dodonov V V 2000 *J. Phys. A: Math. Gen.* **33** 3209
- [18] de la Llave R and Petrov N P 1999 *Phys. Rev. E* **59** 6637
- [19] Ford L H and Vilenkin A 1982 *Phys. Rev. D* **25** 2569
- [20] Barton G and Eberlein C 1993 *Ann. Phys., NY* **227** 222
- [21] Maia Neto P A 1994 *J. Phys. A: Math. Gen.* **27** 2167
- [22] Mundarain D F and Maia Neto P A 1998 *Phys. Rev. A* **57** 1379
- [23] Crocce M, Dalvit D A R and Mazzitelli F D 2001 *Phys. Rev. A* **64** 013808
- [24] Dodonov V V 1995 *Phys. Lett. A* **207** 126
- [25] Dodonov A V, Dodonov E V and Dodonov V V 2003 *Phys. Lett. A* **317** 378
- [26] Dodonov A V and Dodonov V V 2001 *Phys. Lett. A* **289** 291
- [27] Crocce M, Dalvit D A R and Mazzitelli F D 2002 *Phys. Rev. A* **66** 033811
- [28] Dodonov V V 1998 *Phys. Lett. A* **244** 517
- [29] Dodonov V V 1998 *Phys. Rev. A* **58** 4147
- [30] Schaller G, Schützhold R, Plunien G and Soff G 2002 *Phys. Lett. A* **297** 81
- [31] Schaller G, Schützhold R, Plunien G and Soff G 2002 *Phys. Rev. A* **66** 023812
- [32] Plunien G, Schützhold R and Soff G 2000 *Phys. Rev. Lett.* **84** 1882
- [33] Schützhold R, Plunien G and Soff G 2002 *Phys. Rev. A* **65** 043820
- [34] Jing H, Shi Q-Y and Wu J-S 2000 *Phys. Lett. A* **268** 174
- [35] Law C K 1995 *Phys. Rev. A* **51** 2537
- [36] Golestanian R and Kardar M 1997 *Phys. Rev. Lett.* **78** 3421
- [37] Cole C K and Schieve W C 2001 *Phys. Rev. A* **64** 023813
- [38] Antunes N D 2003 *Preprint hep-ph/0310131 v1*
- [39] Li L and Li B Z 2002 *Phys. Lett. A* **300** 27
- [40] Fedotov A, Narozhny N and Lozovik Y 2005 *J. Opt. B: Quantum Semiclass. Opt.* **7** S64
- [41] Ruser M 2005 *J. Opt. B: Quantum Semiclass. Opt.* **7** S100
- [42] Cartier C, Durrer R and Ruser M 2005 *Phys. Rev. D* **72** 104018
- [43] Ruser M 2005 *Preprint quant-ph/0509030*
- [44] <http://www.gnu.org/software/gsl/>